Chapter 2

Experimental Methods and Characterization Techniques for Dye Sensitized Solar Cells

This Page is intentionally left blank

2.1 X-Ray Diffraction analysis

X-ray diffraction (XRD) analysis is a technique used to determine the crystal structure of materials in the nanomaterial, thin-film, or bulk material form. In the XRD experiment, a monochromatic X-ray beam is allowed to incident on the sample and the diffraction occurs. Constructive interference is obtained for the glancing angles (θ) corresponding to those (hkl) planes only for which the path difference is equal to the integral multiple (n) of wavelength (λ) of the X-ray used. This condition is given by Bragg's equation

$$2\,d\,Sin\theta\ =\ n\,\lambda \tag{2.1}$$

where d is the interplanar spacing. The schematic diagram of the experimental arrangement is shown in Fig. 2.1. The reflected X-rays make an angle of 2θ with the material surface. A typical XRD pattern consists of these reflection peaks along the y-axis with the diffraction angles 2θ along the x-axis [1, 2].

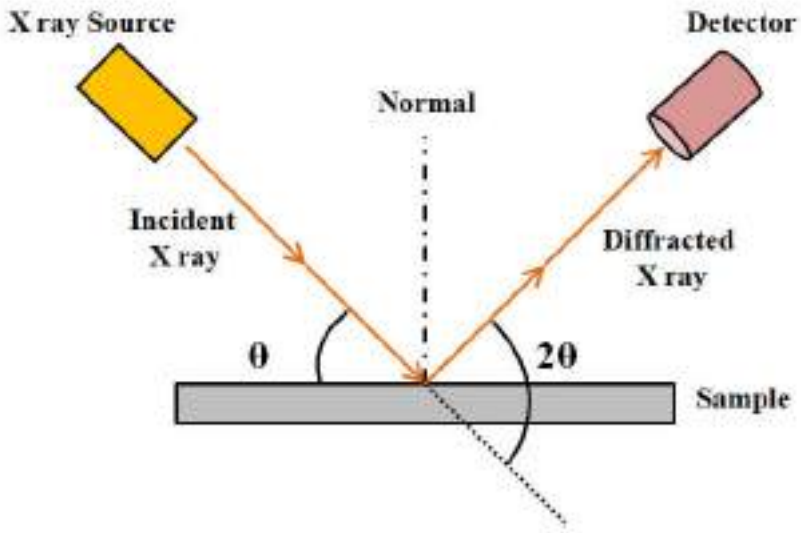

Figure 2.1 X-ray diffraction at the sample film surface.

X-rays are diffracted at specific angles by different crystal planes in nanostructures satisfying Bragg's condition. One can also calculate the inter-planer spacing by knowing θ and λ. XRD is usually performed in the θ- 2θ scan mode where a monochromatic X-ray beam is incident on the nanostructure sample surface. X-ray source and detector motion are coupled with each other so that the detector always makes an angle 2θ with the incidence direction. Finally, the output is plotted as a graph between the recorded intensity of the diffracted beam and angle 2θ. The crystalline size (D) of the sample may be calculated using the Scherrer's formula

$$D = \frac{k\,\lambda}{\beta\,cos\theta} \tag{2.2}$$

Where k ≈ 0.9 and β = Full Width at Half Maximum (FWHM)

In our study, the X-ray diffraction analysis was employed using PAN-analytical X'Pert PRO X-ray diffractometer (CuKα radiation, 30 mA, 40 kV, λ= 1.5406 Å) to determine the crystalline structure and phase of different nanoparticle samples used in making the photoanode of the DSSCs.

2.2 Scanning Electron Microscopy (SEM)

A scanning electron microscope (SEM) [3-6] is a microscope that creates an image by using electrons rather than light. There are numerous advantages to using a scanning electron microscope over a traditional microscope. The SEM has a large depth of field, allowing for more of a specimen to be in focus at once. As the SEM uses electromagnets instead of optical lenses, the researcher has much more control over the magnification level. Along with that, SEM allows much higher resolution compared to optical microscopes. Because of these advantages, the scanning electron microscope is one of the most helpful research tools available today. An electron gun produces an electron beam at the top of the microscope. The electron beam is focused on the sample with the help of electromagnetic lenses. Electrons and

X-rays are emitted once the incident electron beam interacts with the sample. Detectors present in the instrument collect these scattered electrons, X-rays and covert them into signal.

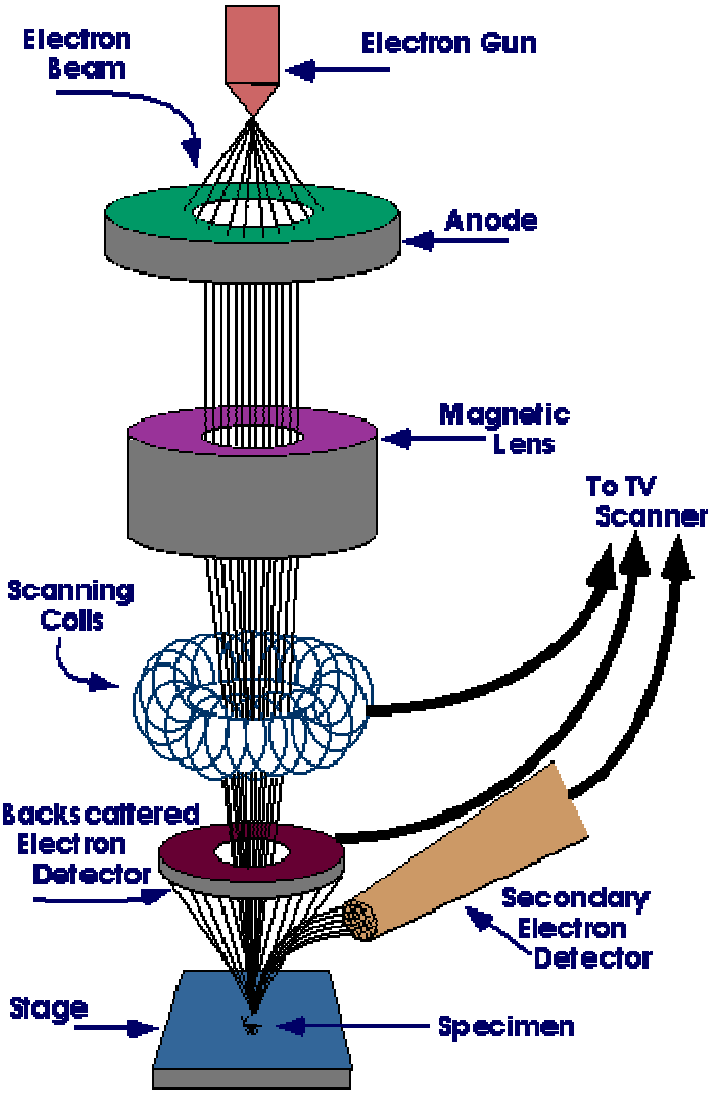

Figure 2.2 Schematic diagram of Scanning Electron Microscope. (https://www.purdue.edu/ehps/rem/laboratory/equipment%20safety/Research%20Equipment/sem.html)

The surface morphology of the sample is exposed by producing a visual image corresponding to the signal received, following the same method with which a picture is created on a television screen.

Figure 2.3 Experimental setup for SEM and EDS measurement.

2.3 UV-VIS spectroscopy

In order to study the absorption spectra of the dye solution, UV-VIS spectroscopy was used. In this measurement, the sample is exposed to light within a selected range of wavelengths. Absorption occurs when the incident photon energy surpasses the energy gap between the lower energy orbital (highest occupied molecular orbital-HOMO) and the higher energy unoccupied orbital (lowest unoccupied molecular orbital-LUMO) of the materials, and then the spectrometer records the signal. The block diagram of the UV-VIS spectrophotometer is shown in Fig. 2.4 [7].

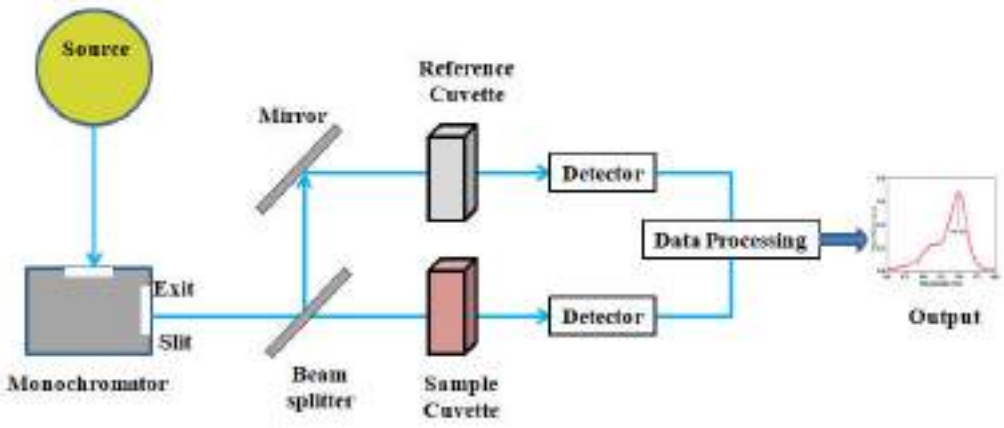

Figure 2.4 Schematic of UV-VIS spectrophotometer.

Figure 2.5 Experimental setup for UV-VIS absorption measurement.

In the present study, the absorbance spectrum measurement of the dye was carried out using a Perkin-Elmer Lambda-35 UV-VIS spectrophotometer.

2.4 Energy Dispersive X-ray spectroscopy (EDS)

Energy Dispersive X-ray Spectroscopy (EDS) study is performed to identify and quantify the elemental composition of the materials [8-10]. The basic working principle of EDS analysis utilizes the interaction of an electron beam with the sample. When primary electrons collide with the sample surface, the inner shell electrons are ejected and X-rays are produced as a result of the transition of the outer shell electrons filling up the vacancy in the inner shell. Due to its unique atomic structure, each element emits a distinct X-ray emission pattern that can be used to perform the atomic compositional analysis of the specimen with an energy dispersive spectrometer. The analysis of these peaks yields both qualitative and semi-quantitative information about the material.

2.5 Raman Spectroscopy

Raman spectroscopy is an analysis technique that measures the vibrational energy modes and provides detailed chemical and structural information about the sample. This information is obtained by detection of the Raman scattering from the sample. When a monochromatic beam of light incident on the sample, most of the scattered light consists frequency same as that of the incident radiation. This is known as Rayleigh scattering. However, a small portion of the scattered light has frequencies above and below the incident frequency which is referred as Raman scattering.

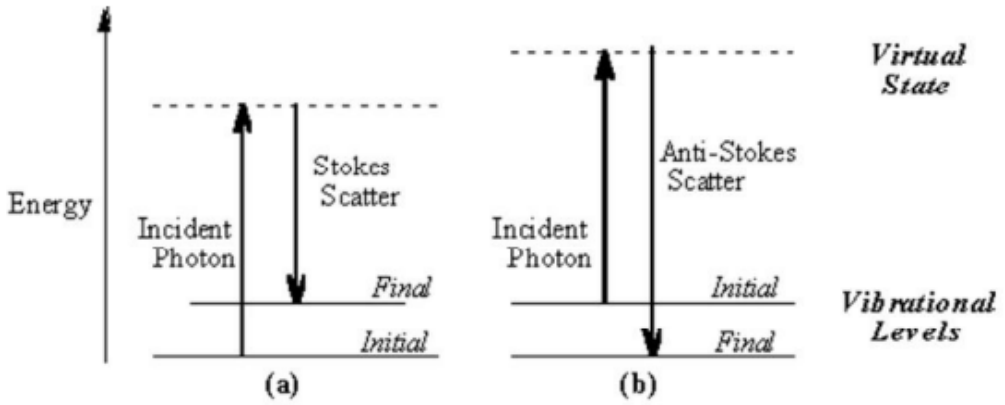

Figure 2.6 (a) Stokes Raman Scattering, (b) Anti-Stokes Raman Scattering.

When a photon beam having energy $h\nu$ suffers an elastic collision with molecules present in the sample, they scatter without suffering any energy exchange with the molecule and thus, the frequency of the scattered light remains unchanged.

However, during the inelastic collision, there will be exchange of energy between the molecule and the photon. Consequently, the scattered light will have a frequency different from the incident frequency. If the molecule absorbs some energy from the incident photon, then it gains some energy and consequently, the scattered photon loses energy. Light scattered with a

frequency lower than the incident frequency is known as Stokes Raman scattering.

On the other hand, when the molecule loses some energy to the scattered photon, the frequency of the scattered light becomes more than the incident light and the corresponding phenomenon is known as Anti-Stokes Raman scattering [11-13].

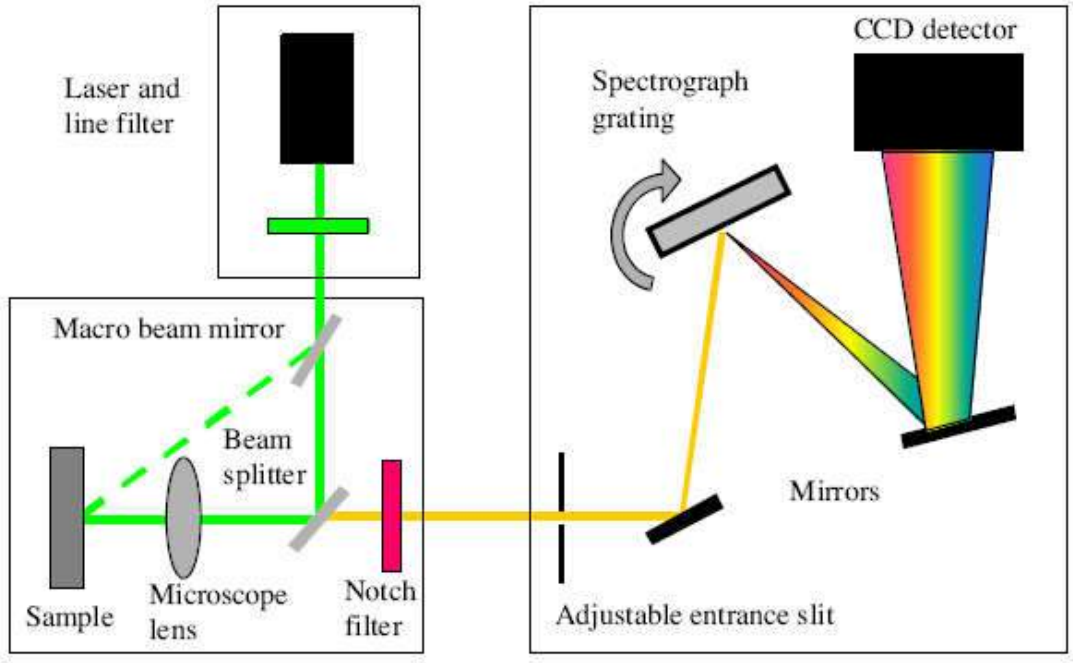

Figure 2.7 Schematic diagram of a typical Raman Spectrophotometer. (https://www.sas.upenn.edu/~crulli/TheRamanSpectrophotometer.html)

In a typical Raman spectrophotometer, a very narrow and monochromatic laser beam (coherent and powerful) is used to excite the target material. Usually, the material is filled inside a narrow quartz or glass tube. The light is scattered by the sample and then collected by a lens. The collected light is passed through a grating Monochromator. Finally, a detector captures the signal and sends it to a computer for decoding.

2.6 Basic parameters to evaluate the performance of DSSCs: Solar Cell Terminologies

Current-voltage measurement is a simple method to evaluate photovoltaic devices under both illumination and dark conditions. Fig. 2.8 represents a simplified equivalent circuit (single diode equivalent model) of a solar cell, including the series (R_s) and parallel resistances (R_{sh}) are added to account for various loss mechanisms a typical I-V curve for a solar cell under illumination and dark.

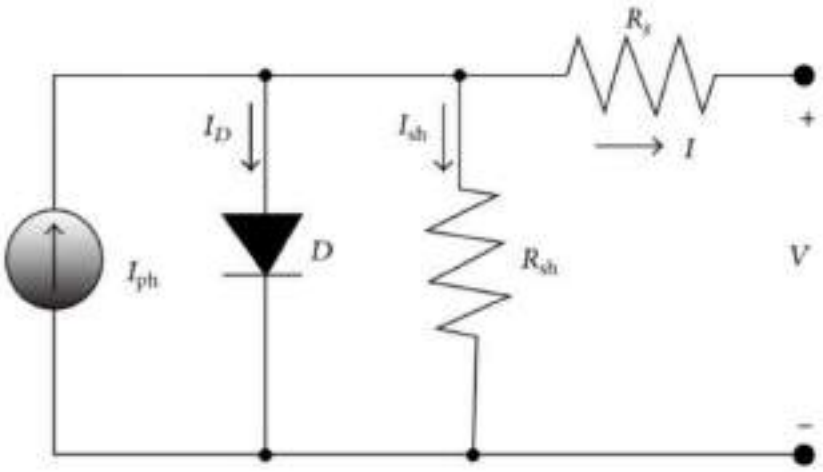

Figure 2.8 One diode equivalent circuit model of a Solar cell [14].

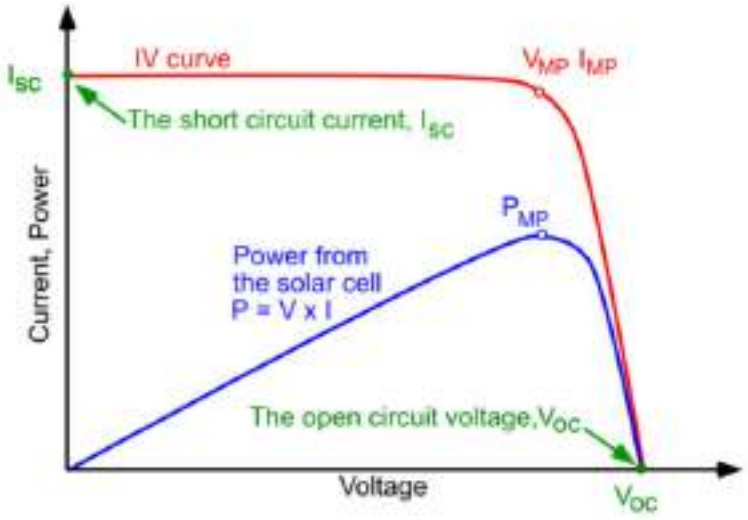

Figure 2.9 Typical I-V characteristics of a solar cell [17].

The current-voltage characteristic of a Solar cell allows us to determine the photovoltaic performance of the cell. The Power-Voltage plot to calculate the maximum power point (P_{MP}), I_{MP} and V_{MP} are represented in Fig. 2.9. Various parameters like photocurrent density (J_{SC}), open-circuit voltage (V_{OC}) and fill factor (FF) can be extracted from the I-V curves. From which the overall photoelectric conversion efficiency (η) can be calculated.

Equivalent circuit modeling is a very important tool required for better understanding and explaining the solar cell performance and analysis of the electrical processes occurring inside the cell. The functioning of a solar cell is generally modeled by a single diode with a constantphoto-generated current source, a series (R_s) and shunt resistance (R_{sh}) as shown in Fig. 2.8. The current-voltage relation is given by the equation

$$I = I_{ph} - I_o \left[exp \left\{ \frac{(q(V + IR_s)}{Ak_BT} \right\} - 1 \right] - \frac{V + IR_s}{R_{sh}} \qquad (2.3)$$

where I_{ph}, I_o, R_s, R_{sh}, q, A, k_B and T are the photocurrent, the saturation current of the diode, the series resistance, the shunt resistance, the electron charge, the ideality factor, the Boltzmann constant, and absolute temperature, respectively [16, 17]. The circuit parameters like R_s and R_{sh} are not directly measurable. They are calculated by fitting the experimental J-V curve with equation 2.3 [15].

Figure 2.10 Experimental Setup for I-V measurement.

2.6.1 Open circuit voltage (V_{OC})

Open-circuit voltage is the maximum voltage obtainable from a solar cell and is obtained when a load with infinite resistance is attached to its terminals i.e. the cell current is zero. It is determined by the difference between the redox potential of the electrolyte and the Fermi level of electrons in the semiconductor, namely TiO_2. For DSSC, V_{oc} is given by:

$$V_{oc} = \frac{E_{CB}}{q} + \frac{kT}{q}\ln\left(\frac{n}{N_{CB}}\right) - \frac{E_{redox}}{q} \quad (volts) \tag{2.4}$$

Where n represents the number of electrons in the TiO_2 conduction band and N_{CB} is the effective density of states [11]. E_{redox} represents the Nernst potential of the redox mediator and first two terms in above equation define the quasi-Fermi level of TiO_2 and.

2.6.2 Short circuit current density (J_{SC})

The short circuit photocurrent (I_{SC}) is the cell photocurrent measured at zero voltage. It is the current obtained from the cell when it is short-circuited or in other words when the load resistance is zero. It largely depends on the photon-generated electrons and the interfacial recombination of the electrons and holes. In general, it is represented in the form of the short circuit current density (J_{SC}) and is defined as $J_{SC}=I_{SC}/A$ (mA/cm^2), Where, A is the effective area of the solar cell. It is a function of the solar illumination, optical properties and charge transfer probability of the cell.

2.6.3 Series Resistance (R_S)

Series resistance, R_s in a solar cell, results from the contact resistance and charge transfer resistance in the semiconductor material. Series resistance reduces the fill factor of the device and thus affects the maximum device power output, while an excessively high value of RS can also reduce the short-circuit current. The open-circuit voltage is not affected by Rs, since at Voc the total current flow through cell itself is zero and hence the series resistance is zero. An approximate value of the series resistance can be determined from the slope of the I-V curve at the open-circuit voltage point.

2.6.4 Shunt Resistance (R_{sh})

Low shunt resistance provides an alternate path for the photo-generated current causing significant power loss. The effect of low shunt resistance is reduced fill factor and lower open-circuit voltage affecting the maximum power output. The short-circuit current is not affected unless for a very low value since at J_{sc} the total current flows through the outer path and hence through the shunt resistance is low. An approximation of the shunt resistance can be calculated from the slope of the I-V curve at the short circuit current point.

2.6.5 Fill Factor (FF)

The fill factor (FF) is a measure of the maximum power output from a solar cell. It represents the squareness of the I-V curve that is The FF describes how a maximum power rectangle fits under the I-V characteristics and is given by the ratio of the maximum output power to the product of I_{SC} and V_{OC} for the solar cell:

$$FF = \frac{I_{MP}V_{MP}}{I_{sc}V_{oc}} \tag{2.5}$$

Where, V_m and I_m are the voltage and current at the maximum power point. Fill factor, being a ratio of the same physical parameters, has no unit. Fill factor is a function of the series and shunt resistance of the solar cell. For DSSC, it reflects the extent of electrical and electrochemical losses during cell operation. To obtain high FF, R_S should be small, while R_{Sh} needs to be as large as possible.

2.6.6 Power Conversion Efficiency (η)

The power conversion efficiency of a photovoltaic cell is described as the ratio of the maximum electrical energy output of the device to the energy input from the sun. Thus the mathematical definition of efficiency is

$$\eta = \frac{P_{out}}{P_{in}} = \frac{I_{sc}V_{oc}FF}{P_{in}} \tag{2.6}$$

Where P_{in} represents the input power of sunlight. Efficiency is generally expressed in percentage. Besides the solar cell performance, it depends on the incident light spectrum and intensity as well as operating temperature. The internationally recognized standard condition for the efficiency measurement of solar cells is under 'AM1.5 Global' solar irradiation and at a temperature of 25°C [18].

2.7 Electrochemical Impedance Spectroscopy (EIS)

The current-voltage measurement of a solar cell is the elementary method to evaluate the overall electro-optical performance of the device. However, it fails to provide detailed information about the limiting factors and resistances offered by the individual components and interfaces of the architecture that inhibit device performance. The electrochemical impedance spectroscopy (EIS) is a very advanced and powerful diagnostic technique that offers simultaneous measurement of various interfacial charge transfer dynamics and recombination mechanisms inside the device. This method is based on analyzing the electrical response of the device to a periodic voltage having variable frequency superimposed on a constant bias potential. These are typically represented by modeling appropriate equivalent circuits in terms of resistors and capacitors [19, 20].

Figure 2.11 Experimental setup for EIS measurement.

2.7.1 Theory of Impedance

The concept of electrical impedance can be realized starting from the theoretical concept of resistance. The electrical resistance of a material

represents the ability of the material to resist the flow of electrical current through it. It is defined by well known Ohm's law as the ratio between voltage (V) and current (I)

$$R = \frac{V}{I} \qquad (2.7)$$

But the applicability of this relationship is restricted to a single circuit element, the ideal resistor. However, most of the systems under investigation contain circuit elements with much more complicated behaviour. This implies that the basic idea of resistance should be replaced by a more general parameter: impedance, which incorporates not only the respective amplitudes of voltage and current but also their relative phases. Impedance is also a measure of a circuit's capacity to resist the flow of electrical current in a specific way, but it isn't restricted to the features of a pure resistance. Impedance is a broad term that refers to the collective obstruction to current offered by resistances, capacitances, and inductances present in the device or the circuit. Typically, electrochemical impedance is analyzed by delivering an alternating potential to an electrochemical cell and measuring the current flowing through it. It is generally measured. In order to produce a linear response from the cell, electrochemical impedance is generally measured by applying a small sinusoidal excitation potential and recording the corresponding current response from the device. This current response will also be a sinusoidal wave with the same frequency but a shifted phase. The applied sinusoidal excitation potential can be represented as

$$V = V_o \sin \omega t \qquad (2.8)$$

The corresponding current response from the device with a shifted phase may be written as

$$I = I_o \ (\sin \omega t + \varphi) \qquad (2.9)$$

where φ is the phase shift. The impedance of the system may be calculated using a formula similar to Ohm's Law.

$$Z = \frac{V}{I} = \frac{V_o \sin \omega t}{I_o \ (\sin \omega t + \ \varphi)} \tag{2.10}$$

It is usually more convenient to represent impedance using complex exponentials. The magnitude and phase of the input and output signals may be represented in a much simpler way using these complex numbers. Furthermore, it provides a more powerful representation for circuit analysis purposes.

The applied potential and current response from the cell can be represented as a complex function having a form like

$$V = V_o \exp(\, j\omega t) \tag{2.11}$$

and $$I = I_o \exp j(\, \omega t - \varphi) \tag{2.12}$$

respectively.

Consequently, the complex impedance may be written as

$$\begin{aligned} Z = \frac{V}{I} = \ & \frac{V_0}{I_0} \exp(j\varphi) \\ & = Z_0 \ (\, cos \ \varphi + j \ sin \ \varphi) \\ & = Z' + j \ Z'' \end{aligned} \tag{2.13}$$

where $Z' = Z_0 \cos \varphi$ and $Z'' = Z_0 \sin \varphi$ are the real and imaginary components of the impedance respectively.

2.7.2 Nyquist and Bode plots

During the impedance measurement, the system is generally kept in a steady condition prior to applying an alternating potential and measuring the corresponding alternating response current through the cell. Globally used impedance measurement setups allow measurement of the complex impedance and phase shift at a particular applied frequency The impedance of the system as a function of frequency may be easily obtained by varying the frequency of the applied signal in a continuous way. Impedance parameters for specific internal components of the cell can be assigned using proper model equivalent circuits (which might have multiple options dependent on splitting an actual

device into component structures). The recorded data is usually represented in two ways; one is the Nyquist plot depicting the plot between real (Z') and imaginary (Z'') part of the impedance and another is the Bode plot depicting the variation of the magnitude of the impedance ($Z_0 = |Z|$) or phase (φ) with frequency (f) of the applied signal as shown in Fig. 2.12 (a) and fig. 2.12 (b) respectively.

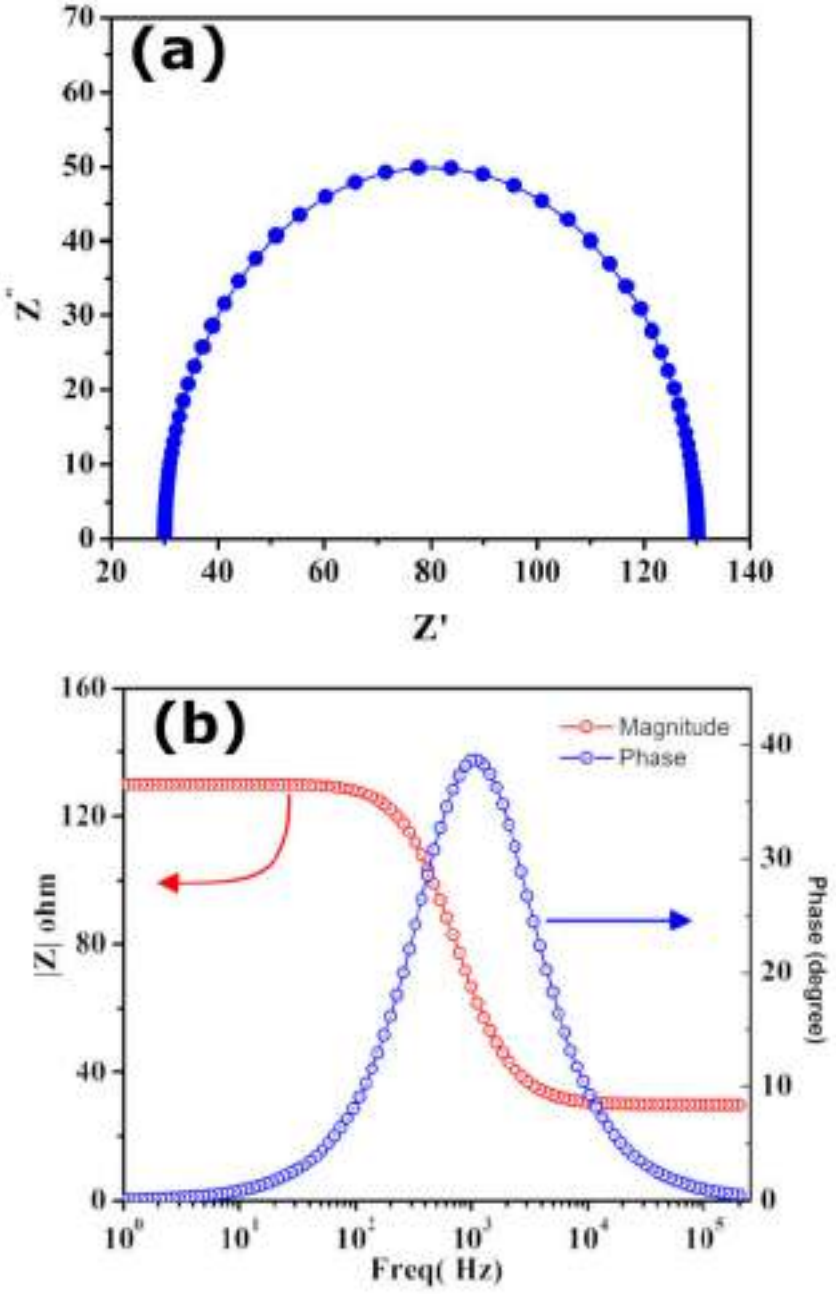

Fig. 2.12 Typical **(a)** Nyquist and **(b)** Bode plot.

2.7.3 Equivalent circuit for impedance measurement of DSSC

A dye-sensitized solar cell is a very complex system, and its ultimate impedance response depends on the responses received from various components of the device. The electronic processes that occur within the DSSC are well represented by the transmission line model developed by Bisquert [21]. The transmission line model widely used to represent different charge transfer, recombination and diffusion processes occurring inside DSSC is shown in Fig. 2.13.

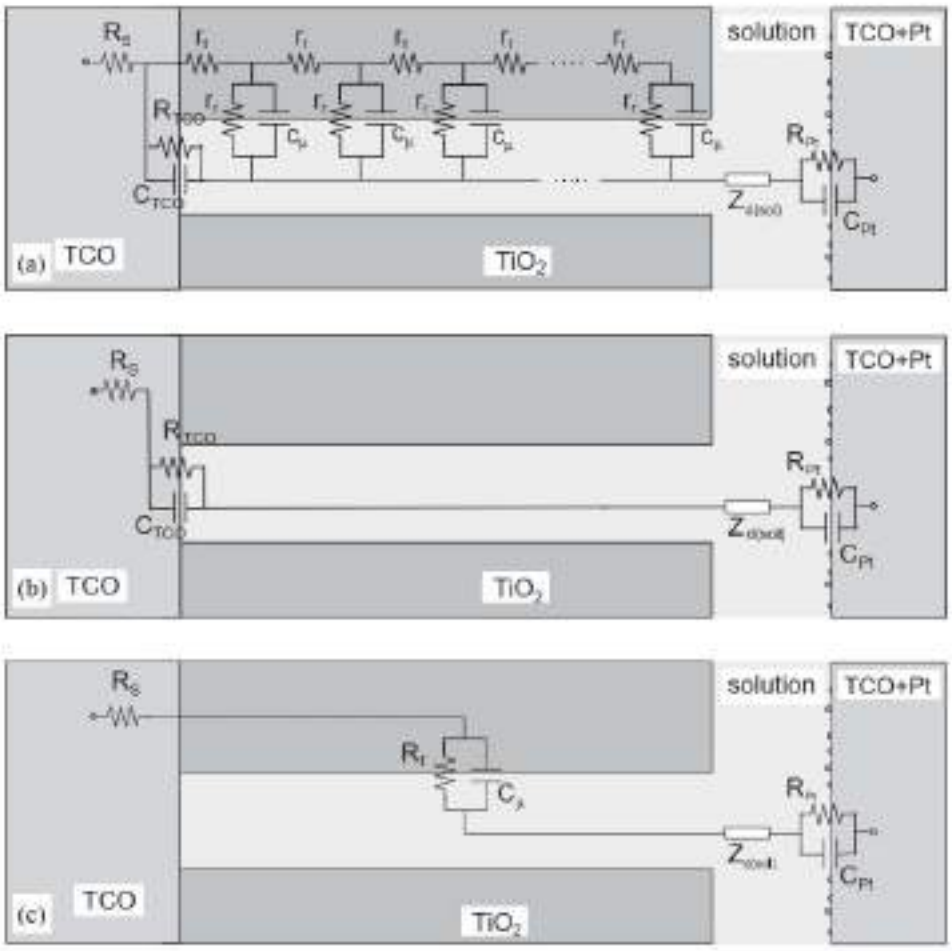

Fig. 2.13 (a) Equivalent circuit for a complete solar cell; (b) Simplified circuit for insulating TiO2 (potentials around 0 V) as currents are low, Z_d may be skipped and (c) Simplified equivalent circuit of a DSSC when the TiO_2 is in conducting state (At V_{oc} bias potential) [22].

Usually, the EIS measurement is carried out at the potentials near to V_{oc} in order to in order to achieve consistency equivalent to that of a real system. The nanostructured oxide model has been simplified to a columnar model in this illustration, which depicts the mesoporous layer through which the electrolyte solution passes. The different circuit elements are:

- R_s is sheet resistance of the TCO layer and contact resistances.
- $R_t = r_t L$ is the electron transport resistance.
- $R_r = r_r/L$ is the charge transfer resistance related to the recombination of the electrons at the TiO_2+dye/electrolyte interface.
- R_{TCO} is the charge-transfer resistance for electron recombination from the uncovered layer of the TCO to the electrolyte.
- C_{TCO} is the capacitance at the triple contact TCO/TiO_2/electrolyte interface
- C_μ is the capacitance at the TiO2+dye/electrolyte interface.
- Z_d(sol) is the impedance of the redox species diffusion into the electrolyte, generally called Nernst impedance Z_N.
- R_{Pt} is the charge transfer resistance at the counter electrode.
- C_{Pt} is the capacitance at the electrolyte/counter electrode interface.

The first three mentioned elements are denoted in lowercase letters in Fig. 2.13(a), meaning the element per unit length for a film of thickness L, because they are distributed in a repetitive arrangement of a transmission line. Physical interpretation of the different electrochemical operations across the interfacial regions of the DSSCs can be made by fitting the EIS spectra with the appropriate equivalent circuit. Generally, a typical Nyquist plot of a DSSC exhibits three semicircles (Fig. 2.14). The first semicircle in the high frequency range (above 100 Hz) describes the charge transfer at the Pt/electrolyte interface (Z_1), the second semicircle at an intermediate frequency range (1-100 Hz) is related to the recombination at the photoanode/electrolyte interface and the charge transport into the semiconductor (Z_2). The third one at low

frequency (below 1 Hz) represents the diffusion in the electrolyte (Z_3) and is attributed to the Nernst contribution. If the voltage is reduced, the two external semicircles are incorporated into the biggest one. Nevertheless, these Nyquist plots have one major limitation: they do not give complete information on the exact frequency used to record one point.

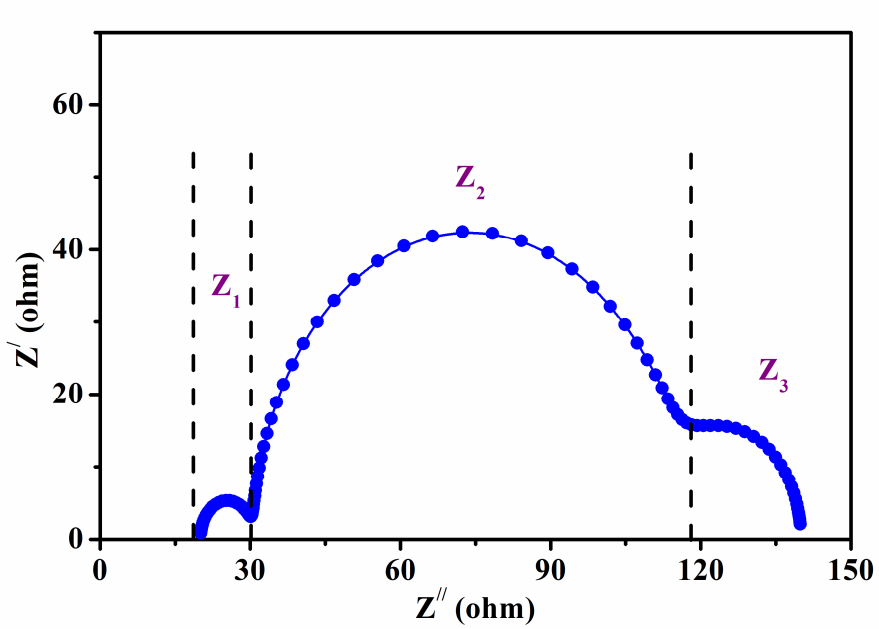

Fig. 2.14 Typical Nyquist plot of a DSSC under Open circuit condition.

Another important representation of the EIS data is Phase bode plot representing Phase (-θ) vs. Frequency (f) curve. Unlike the Nyquist plot, the very important aspect of this plot is that frequency information is not lost.

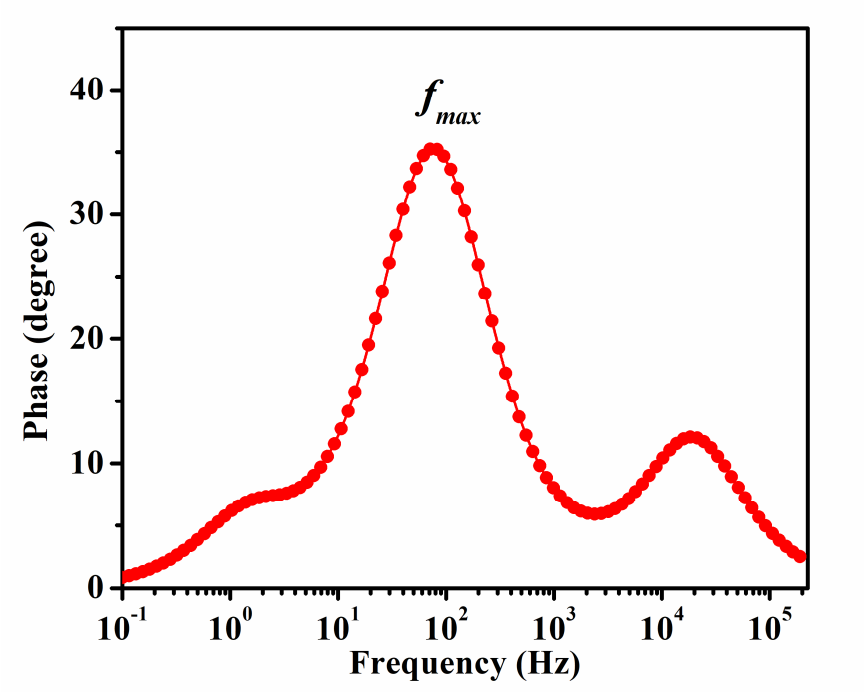

Fig. 2.15 Typical Bode plot (Phase) representation of a DSSC.

The average carrier lifetime can be estimated from phase bode plots (shown in Fig. 2.15) using the formula

$$\tau_e = \frac{1}{2\pi f_{max}}$$

where f_{max} represents peak frequency in the mid-frequency range [23].

References:

[1] Epp, J.: X-ray diffraction (XRD) techniques for materials characterization. In Materials characterization using nondestructive evaluation (NDE) methods (pp. 81-124) (2016). Woodhead Publishing.

[2] Zhang, L. Z., & Tang, G. Q. :Preparation, characterization and optical properties of nanostructured ZnO thin films. Optical Materials, 27(2), 217-220(2004).

[3] Vernon-Parry, K. D. "Scanning electron microscopy: an introduction." III-Vs Review 13, no. 4 (2000).

[4] McMullan, D. "Scanning electron microscopy 1928–1965." Scanning 17, no. 3 (1995): 175-185.

[5] Zhou, Weilie, Robert Apkarian, Zhong Lin Wang, and David Joy. "Fundamentals of scanning electron microscopy (SEM)." In Scanning microscopy for nanotechnology, pp. 1-40. Springer, New York, NY, 2006.

[6] Goldstein, Joseph I., Dale E. Newbury, Joseph R. Michael, Nicholas WM Ritchie, John Henry J. Scott, and David C. Joy. Scanning electron microscopy and X-ray microanalysis. Springer, 2017.

[7] Rocha, F. S., Gomes, A. J., Lunardi, C. N., Kaliaguine, S., & Patience, G. S.: Experimental methods in chemical engineering: Ultraviolet visible spectroscopy—UV-Vis. The Canadian Journal of Chemical Engineering, 96(12), 2512-2517(2018).

[8] d'Alfonso, A. J., B. Freitag, D. Klenov, and L. J. Allen. "Atomic-resolution chemical mapping using energy-dispersive x-ray spectroscopy." Physical Review B 81, no. 10 (2010): 100101.

[9] Allen, Leslie J., Adrian J. D'Alfonso, Bert Freitag, and Dmitri O. Klenov. "Chemical mapping at atomic resolution using energy-dispersive x-ray spectroscopy." MRS bulletin 37, no. 1 (2012): 47-52.

[10] Shindo, Daisuke, and Tetsuo Oikawa. "Energy dispersive x-ray spectroscopy." In Analytical electron microscopy for materials science, pp. 81-102. Springer, Tokyo, 2002.

[11] Long, Derek Albert. "Raman spectroscopy." New York 1 (1977).

[12] Larkin, Peter. Infrared and Raman spectroscopy: principles and spectral interpretation. Elsevier, 2017.

[13] Koningstein, Johannes Arnoldus. Introduction to the Theory of the Raman Effect. Springer Science & Business Media, 2012.

[14] Ma, Jieming, Ka Lok Man, T. O. Ting, Nan Zhang, Sheng-Uei Guan, and Prudence WH Wong. "Approximate single-diode photovoltaic model for efficient IV characteristics estimation." The Scientific World Journal 2013 (2013).

[15] Cotfas, D. T., P. A. Cotfas, and S. Kaplanis. "Methods to determine the dc parameters of solar cells: A critical review." Renewable and Sustainable Energy Reviews 28 (2013): 588-596.

[16] Murayama, Masaki, and Tatsuo Mori. "Equivalent circuit analysis of dye-sensitized solar cell by using one-diode model: effect of carboxylic acid treatment of TiO2 electrode." Japanese journal of applied physics 45, no. 1S (2006): 542.

[17] Charles, J. P., M. Abdelkrim, Y. H. Muoy, and P. Mialhe. "A practical method of analysis of the current-voltage characteristics of solar cells." Solar cells 4, no. 2 (1981): 169-178.

[18] Smestad, Greg P., Frederik C. Krebs, Carl M. Lampert, Claes G. Granqvist, K. L. Chopra, Xavier Mathew, and Hideyuki Takakura. "Reporting solar cell efficiencies in solar energy materials and solar cells." Solar Energy Materials and Solar Cells 92, no. 4 (2008): 371-373.

[19] Fabregat-Santiago, Francisco, Juan Bisquert, Emilio Palomares, Luis Otero, Daibin Kuang, Shaik M. Zakeeruddin, and Michael Grätzel. "Correlation between photovoltaic performance and impedance

spectroscopy of dye-sensitized solar cells based on ionic liquids." The Journal of Physical Chemistry C 111, no. 17 (2007): 6550-6560.

[20] Hagfeldt, Anders, Gerrit Boschloo, Licheng Sun, Lars Kloo, and Henrik Pettersson. "Dye-sensitized solar cells." Chemical reviews 110, no. 11 (2010): 6595-6663.

[21] Bisquert, Juan. "Theory of the impedance of electron diffusion and recombination in a thin layer." The Journal of Physical Chemistry B 106, no. 2 (2002): 325-333.

[22] Fabregat-Santiago, Francisco, Juan Bisquert, Germà Garcia-Belmonte, Gerrit Boschloo, and Anders Hagfeldt. "Influence of electrolyte in transport and recombination in dye-sensitized solar cells studied by impedance spectroscopy." Solar energy materials and solar cells 87, no. 1-4 (2005): 117-131.

[23] Bhatt, Parth, Kavita Pandey, Pankaj Yadav, Brijesh Tripathi, and Manoj Kumar. "Impedance spectroscopic investigation of the degraded dye-sensitized solar cell due to ageing." International Journal of Photoenergy 2016 (2016).

This Page is intentionally left blank